Colloidal synthesis and blue based multicolor upconversion emissions of size and composition controlled monodisperse hexagonal $NaYF_4$: Yb,Tm nanocrystals†

Anxiang Yin, Yawen Zhang,* Lingdong Sun and Chunhua Yan*

Received (in Hong Kong, China) 9th December 2009, Accepted 4th February 2010
First published as an Advance Article on the web 29th March 2010
DOI: 10.1039/b9nr00397e

Monodisperse β-$NaYF_4$: Yb,Tm nanocrystals with controlled size (25–150 nm), shape (sphere, hexagonal prism, and hexagonal plate), and composition (Yb: 20–40%, Tm: 0.2–5%) were synthesized from the thermolysis of metal trifluoroacetates in hot surfactant solutions. The upconversion (UC) of near-infrared light (980 nm) to ultra-violet (360 nm), blue (450 and 475 nm), red (650 and 695 nm) and infrared (800 nm) light in the β-$NaYF_4$: Yb,Tm nanocrystals has been studied by UC spectroscopy. Both the total intensity of UC emissions and the relative intensities of emissions at different wavelengths have shown a strong dependence on different particle sizes and different Tm^{3+} and Yb^{3+} concentrations. As a result, different overall output colors of UC emissions can be achieved by altering sizes and Yb^{3+}/Tm^{3+} doping concentrations of the β-$NaYF_4$: Yb,Tm nanocrystals. The intensity-power curves of a series of samples have proved that emissions at 360 and 450 nm can be ascribed to four-photon process ($^1D_2$ to $^3H_6$ and $^1D_2$ to $^3H_4$, respectively), while emissions at 475 and 650 nm are three-photon processes ($^1G_4$ to $^3H_6$ and $^1G_4$ to $^3H_4$, respectively) and emissions at 695 and 800 nm are two-photon ones ($^3F_2$ to $^3H_6$ and $^3F_4$ to $^3H_6$, respectively). A UC saturation effect would occur under a certain excitation intensity of the 980 nm CW diode laser for the as-obtained β-$NaYF_4$: Yb,Tm nanocrystals, leading to the decrease of the slopes of the *I–P* curves. The results of our study also revealed that the successive transfer model instead of the cooperative sensitization model can be applied to explain the UC behaviors of the β-$NaYF_4$: Yb,Tm nanocrystals. Further, an unexpected stronger emissions of four-photon process at 360 and 450 nm for ~50 nm β-$NaYF_4$: Yb,Tm nanocrystals than those for the bigger (~150 nm) nanocrystals was observed and explained in terms of the effects of crystallite size, surface-to-volume ratio and homogeneity of the doping cations.

Introduction

Upconversion (UC) phosphors, especially rare-earth-based (RE-based) UC phosphors, have been a hotspot of material research for several decades because of their wide and important applications in many realms, such as solid-state lasers, IR imaging[1,2] and bioimaging.[1c,3] Compared to those traditional biological labels, for example, organic dyes[4] and semiconductors,[5] RE-based UC fluorescent (from near-infrared (NIR) to visible) nanoparticles possess several inherent advantages, including weak autofluorescence backgrounds, strong penetration abilities for NIR radiation, resistances to photobleaching, and low toxicity, *etc*.[4,5,6] Among those UC materials, β-$NaYF_4$ is considered to be one of the most efficient host materials for green/blue UC phosphors when sensitized by Yb^{3+} and activated by Er^{3+}/Ho^{3+}/Tm^{3+} ions due to the relatively low lattice phonon energy.[1,7]

More recently, much attention has been focused on the size/shape/phase-controlled synthesis, UC properties and mechanisms, and bio-applications of the $NaYF_4$: Yb,Er/Tm nanocrystals.[8] For instance, Haase and co-workers[8a] reported the precipitation-based solution synthesis of $NaYF_4$: Yb,Er/Tm nanoparticles with bright UC emissions, revealing the application potential of UC nanocrystals in bio-imaging areas. Li *et al.*[8b,i] obtained $NaYF_4$ nanocrystals with controllable size and morphology and high dispersibility by hydrothermal procedures. Yan *et al.*,[8c] Capobianco *et al.*,[8d,e] and Chow *et al.*[8f] developed the method of thermal decomposition of metal–organic complexes in hydrophobic high-boiling solvents to synthesize monodisperse $NaYF_4$: Yb,Er/Tm nanocrystals with controllable size, shape and phase. Yan *et al.*[8j,k] also studied the nucleation and growth kinetics, and multicolor UC emissions and mechanisms of $NaYF_4$: Yb,Er nanocrystals, revealing the relationships between the outcome UC emissions and size, shape, phase and composition of the nanocrystals. Liu and co-workers[1c,9a] realized the tuning of the outcome UC light color of $NaYF_4$: Yb,Er nanocrystals *via* incorporating Tm^{3+} cations and altering the doping concentrations. Veggel *et al.*[9f] obtained transparent UC NPs-polymer composite materials *via*

Beijing National Laboratory for Molecular Sciences, State Key Laboratory of Rare Earth Materials Chemistry and Applications, PKU-HKU Joint Laboratory in Rare Earth Materials and Bioinorganic Chemistry, Peking University, Beijing, 100871, China. E-mail: yan@pku.edu.cn; ywzhang@pku.edu.cn; Fax: +86-10-6275-4179; Tel: +86-10-6275-4179

† Electronic supplementary information (ESI) available: More TEM images and UC results of the β-$NaYF_4$: Yb,Tm nanocrystals. See DOI: 10.1039/b9nr00397e

dispersing $NaYF_4$ nanoparticles into PMMA through an *in situ* polymerization method. Zhang and co-workers[9b] employed $NaYF_4$: Yb,Er@SiO_2 as fluorescent labels in cell imaging. Also, they achieved multicolor UC fluorescence by using $NaYF_4$: Yb,Er nanocrystals as the energy donator in the FRET process to organic dyes and QDs.

Compared to the massive studies on the $NaYF_4$: Yb,Er nanocrystals with green UC emissions, researches on the $NaYF_4$: Yb,Tm nanocrystals with blue emissions are still scarce, though they are important and necessary supplement to the NIR to visible light UC nanomaterials. For example, Nann *et al.*[9d] exploited $NaYbF_4$: Tm nanocrystals as one of the probes for multiplexing detections. Zhang *et al.* studied the core–shell effects[9b] and the bio-applications[9c] of $NaYF_4$: Yb,Er and $NaYF_4$: Yb,Tm nanocrystals. Prasad *et al.*[9e] introduced $NaYF_4$: Yb,Tm nanoparticles as an *in vitro* and *in vivo* NIR-NIR UC probes. Further compared to the systematic studies of UC emissions and mechanisms of bulk $NaYF_4$: Yb,Tm materials,[11] the fundamental understanding of the size/shape/phase modulated UC properties and mechanisms of $NaYF_4$: Yb,Tm nanocrystals is still rather inadequate.

In this article, we report the controlled synthesis, tuning of the UC emission colors, and the inherent UC mechanisms of monodisperse $NaYF_4$: Yb,Tm nanocrystals with different dopant ratios (Yb: 20–40%, Tm: 0.2–5%), sizes (25–150 nm), and shapes (sphere, hexagonal prism, and hexagonal plate).

Experimental section

A Schlenk line system and commercially available reagents were used in the synthesis procedure. Rare-earth oxides (RE = Y, Yb, and Tm), oleic acid (OA; 90%, Alpha), oleylamine (OM; >80%, Acros), 1-octadecene (ODE; >90%, Acros), trifluoroacetic acid (99%, Acros), CF_3COONa (>97%, Acros), absolute ethanol, and cyclohexane were used as received. $RE(CF_3COO)_3$ were prepared *via* the literature method.[8c,10]

Synthesis of α-$NaYF_4$: Yb,Tm nanocrystals

1 mmol of CF_3COONa and the appropriate proportion of $Y(CF_3COO)_3$, $Yb(CF_3COO)_3$, and $Tm(CF_3COO)_3$ were added to a mixed solution of OA (10 mmol), OM (10 mmol), and ODE (20 mmol) in a three-necked flask at room temperature. Then, the slurry was degassed and heated to 140 °C with vigorous magnetic stirring for 30 min in a temperature-controlled electromantle to remove water and oxygen, and thus to form an optically transparent, colorless or slightly yellow solution. Next, the solution was heated to 300 °C at a heating rate of 20 °C min^{-1} under a high purified N_2 atmosphere. The solution became a bit turbid and was maintained at this temperature for 30 min under N_2 atmosphere. The solution was left to be air-cooled with gentle stirring for 5–10 min after it became transparent again. Then, an excess amount of ethanol was poured into the solution at room temperature. The resultant turbid mixture was separated by a centrifuge; and the products were collected. The as-precipitated nanocrystals, without any size-selections, were washed several times with cyclohexane and ethanol, and then dried at 80 °C in air for 24 h.

Synthesis of β-$NaYF_4$: Yb,Tm nanocrystals

The synthesis procedure of β-$NaYF_4$: Yb,Tm nanocrystals was similar to the synthesis of α-$NaYF_4$: Yb,Tm nanocrystals except that (a) quantitative CF_3COONa and α-$NaYF_4$:Yb,Tm nanocrystals were added to a mixed solution of OA (20 mmol), and ODE (20 mmol) and, (b) the reaction temperature was increased to 320–330 °C and maintained for 30–45 min (see Table S1 in the ESI†). These obtained nanocrystals could be easily redispersed in various nonpolar organic solvents (*e.g.*, cyclohexane) and showed good redispersibility even after aging for a long time.

Instrumentation

X-ray diffraction (XRD) patterns of the dried powders were recorded on a Rigaku D/MAX-2000 diffractometer (Japan) with a slit of 1/2° at a scanning rate of 4° min^{-1} using Cu-Kα radiation (λ = 1.5418 Å). Samples for transmission electron microscopy (TEM) analysis were prepared by drying a drop of colloid solution of $NaYF_4$: Yb,Tm nanocrystals in cyclohexane on copper grids coated by amorphous carbon. Particle sizes and shapes were examined by a TEM (200CX, JEOL, Japan) operated at 160 kV. High resolution TEM (HRTEM) and EDS analysis was performed on a FEG-TEM (Tecnai F30, Philips, USA) operated at 300 kV. UC emission spectra of all samples (1 wt % $NaYF_4$: Yb,Tm nanocrystal dispersion in cyclohexane) were measured on a Raman spectrometer (Jobin-Yvon HR800, France) with an external tunable 2 W 980 nm diode laser as the excitation source under the same conditions.

Results and discussion

1. Characteristics of β-$NaYF_4$: Yb,Tm nanocrystals

High-quality β-$NaYF_4$: Yb,Tm nanocrystals (nanospheres, hexagonal nanoprisms, and hexagonal nanoplates) in a pure hexagonal structure (space group: $P\bar{6}$) with different Yb and Tm

Table 1 Molar ratio, size, crystal structure, space group and morphology of the as-obtained β-$NaYF_4$: Yb,Tm nanocrystals

Molar ratio[a]					
Yb (%)	Tm (%)	Size/nm[b]	Structure	Space group	Morphology
30	0.2	24.4 ± 1.2	Hexagonal	$P\bar{6}$	Sphere
	0.5	23.9 ± 0.8	Hexagonal	$P\bar{6}$	Sphere
		47.3 ± 1.7	Hexagonal	$P\bar{6}$	Hexagonal prism
		150 × 70	Hexagonal	$P\bar{6}$	Hexagonal plates
	1	24.1 ± 0.8	Hexagonal	$P\bar{6}$	Sphere
	2	24.4 ± 1.0	Hexagonal	$P\bar{6}$	Sphere
	5	24.5 ± 0.8	Hexagonal	$P\bar{6}$	Sphere
20	0.2	23.7 ± 0.7	Hexagonal	$P\bar{6}$	Sphere
	0.5	25.4 ± 1.0	Hexagonal	$P\bar{6}$	Sphere
	1	22.8 ± 0.8	Hexagonal	$P\bar{6}$	Sphere
	2	23.6 ± 0.8	Hexagonal	$P\bar{6}$	Sphere
	5	23.9 ± 0.6	Hexagonal	$P\bar{6}$	Sphere
40	0.2	23.9 ± 0.8	Hexagonal	$P\bar{6}$	Sphere
	0.5	23.1 ± 0.9	Hexagonal	$P\bar{6}$	Sphere
	1	24.2 ± 1.0	Hexagonal	$P\bar{6}$	Sphere
	2	25.2 ± 0.9	Hexagonal	$P\bar{6}$	Sphere
	5	24.4 ± 1.0	Hexagonal	$P\bar{6}$	Sphere

[a] Molar ratio of reactants. [b] The standard deviation statistic from at least 50 particles.

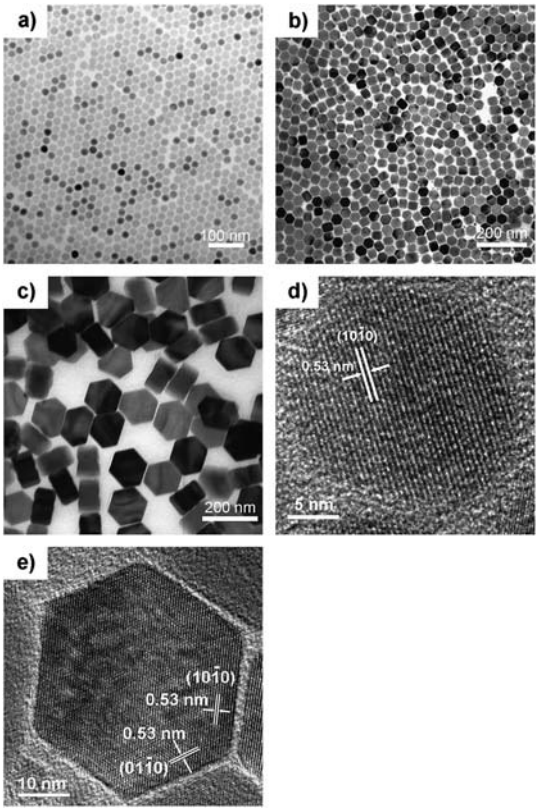

Fig. 1 TEM images of β-$NaYF_4$: 30%Yb,0.5%Tm nanocrystals of different sizes and shapes: (a) 23.9 ± 0.8 nm nanospheres; (b) 47.3 ± 1.7 nm nanoprisms; and (c) ~150 nm × ~70 nm nanoplates. HRTEM images of β-$NaYF_4$: 30%Yb,0.5%Tm nanocrystals: (d) 23.9 ± 0.8 nm nanospheres; (e) 47.3 ± 1.7 nm nanoprisms.

concentrations and different sizes ranging from 25 to 150 nm were selectively synthesized under 320–330 °C for 30–45 min, with using α-$NaYF_4$: Yb,Tm as the seeds and CF_3COONa as the fluorine source (Table 1 and Table S1†). In the present synthesis, the transformation from the α-$NaYF_4$: Yb,Tm seeds to the β-$NaYF_4$: Yb,Tm nanocrystals was realized under the presence of excess Na^+ and F^- ions controllably released from CF_3COONa.[8j,k]

Shapes and sizes of β-$NaYF_4$: Yb,Tm nanocrystals were revealed by TEM measurements. All the obtained β-$NaYF_4$: Yb,Tm nanocrystals showed high size- and shape-uniformity. Small nanocrystals, with the size of about 25 nm, were all of the shape of sphere (for a typical example, see Fig. 1a), while those larger nanocrystals possessed the shape of hexagonal prisms (about 50 nm; Fig. 1b) or hexagonal plates (about 150 nm × 70 nm; Fig. 1c). Powder X-ray diffraction patterns (Fig. 2) were in good agreement with the JCPDS data (JCPDS Card #: 16–0334), revealing that all these nanocrystals are of hexagonal phase with the $P\bar{6}$ symmetry; while HRTEM images (Fig. 1d and e) showed that both the ~25 nm spheres and the ~50 nm prisms are all single crystalline. More TEM images of as-synthesized β-$NaYF_4$: Yb,Tm nanocrystals with different Yb^{3+}/Tm^{3+} concentrations are provided in the ESI† (see Fig. S1). EDS analysis of some typical samples reveal that the concentrations of different RE cations in the final nanocrystalline products agree well with the original molar ratios of the metal precursors (see Table 2),

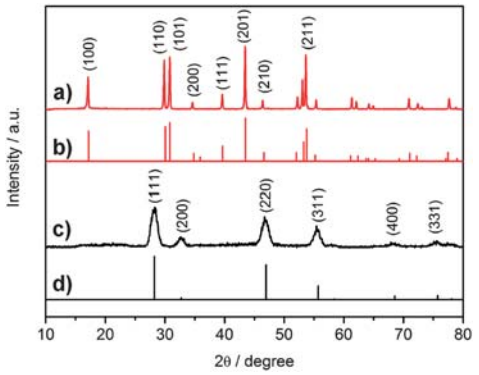

Fig. 2 XRD pattern of (a) as-obtained β-$NaYF_4$: 30%Yb,0.5%Tm nanocrystals (47.3 ± 1.7 nm nanoprisms); (b) JCPDS Card # 16–0334; (c) as-obtained α-$NaYF_4$: Yb,Tm nanocrystals, and (d) JCPDS Card # 77–2042.

Table 2 EDS characterization of β-$NaYF_4$: Yb,Tm nanocrystals

Molar ratio[a]			EDS results (atomic ratio)[b]		
Yb (%)	Tm (%)	Size/nm	Y (%)	Yb (%)	Tm (%)
20	0.5	25.4 ± 1.0	79.6	19.8	0.6
30	0.5	23.9 ± 0.8	68.2	31.2	0.6
		47.3 ± 1.7	69.3	30.1	0.6
	1	24.1 ± 0.8	72.2	26.8	1.1
	2	24.4 ± 1.0	64.1	33.5	2.3
40	0.5	23.1 ± 0.9	61.9	37.4	0.7

[a] Molar ratio of reactants. [b] Average of three independent areas on the copper grid for each sample.

indicating that quantitative doping of Yb^{3+} and Tm^{3+} ions into $NaYF_4$ lattice was achieved by the present synthesis method.

2. UC properties of β-$NaYF_4$: Yb,Tm nanocrystals

2.1. UC emissions of β-$NaYF_4$: Yb,Tm nanocrystals. As shown in Fig. 3a, in the case of β-$NaYF_4$: 30%Yb,0.5%Tm nanocrystals, the near-ultra-violet to visible emission bands of the UC spectra of Yb^{3+}/Tm^{3+} transitions include 360 ($^1D_2$ – $^3H_6$), 450 ($^1D_2$ – $^3H_4$), 475 ($^1G_4$ – $^3H_6$), 650 ($^1G_4$ – $^3H_4$) and 695 nm ($^3F_2$ – $^3H_6$). The infrared emission at around 800 nm is much stronger than those of ultra-violet and visible light, which enables the as-obtained β-$NaYF_4$: Yb,Tm nanocrystals to be excellent candidates for NIR-NIR bioprobes[9d] (Fig. 3b and Fig. S2 of the ESI†).

2.2. UC emissions of β-$NaYF_4$: Yb,Tm nanocrystals with different doping ratios of Yb^{3+} and Tm^{3+}. In the research work of bulk GdF_3 : Yb,Tm[11a] and YF_3 : Yb,Tm[11b] materials, Hewes *et al.*[11a] and Ostermayer *et al.*[11b] studied the UC luminescence mechanism of Yb^{3+} and Tm^{3+} system, pointing out the four-, three- and two-photon processes involved in the UC light and the effects of different doping ratios of Yb and Tm cations on the UC emissions.

The UC excitation and emission behavior of as-synthesized β-$NaYF_4$: Yb,Tm nanocrystals are similar to those of bulk materials, and can be also artificially altered by changing different doping ratios. As seen from Fig. 4a, the UC intensities

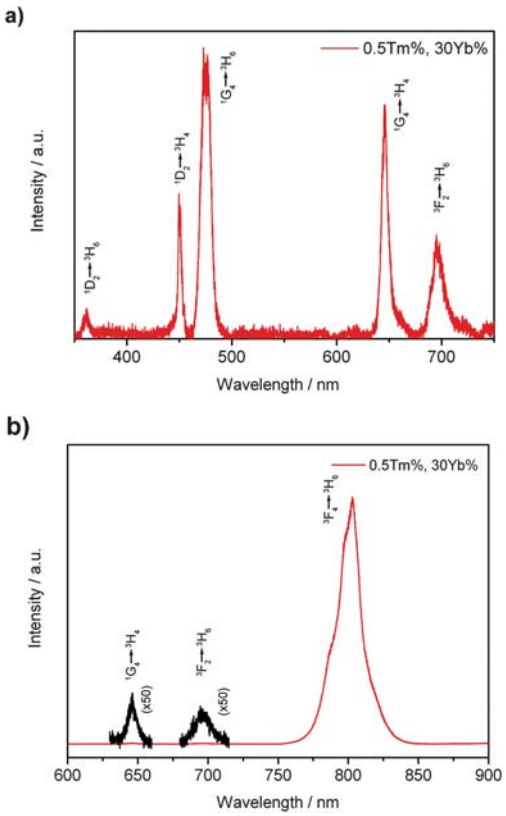

Fig. 3 UC spectra of β-$NaYF_4$: 30%Yb,0.5%Tm nanocrystal dispersion (23.9 ± 0.8 nm) in cyclohexane (1 wt%) pumped by a 980 nm laser: (a) UV and visible emissions and (b) red and IR emissions.

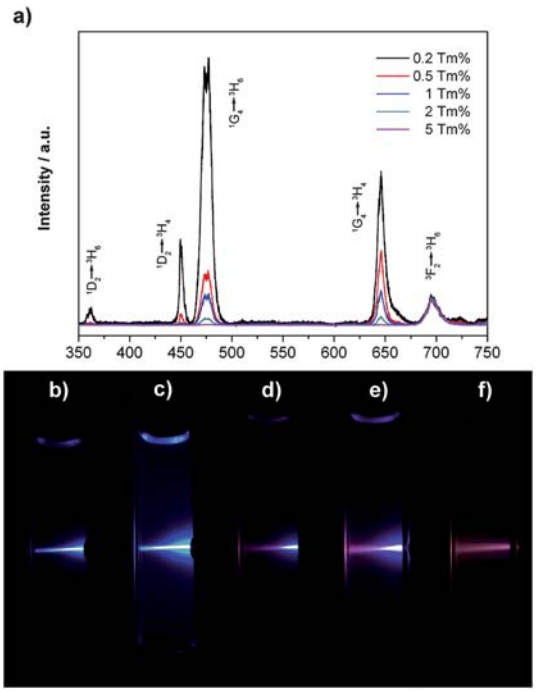

Fig. 4 UC spectra of β-$NaYF_4$: 20%Yb,0.2–5%Tm nanocrystal dispersions (~25 nm) in cyclohexane (1 wt%), normalized at the emission peak of ~695 nm (a); and digital photos of the UC photoluminescence of the β-$NaYF_4$: 20%Yb,0.2–5%Tm nanocrystal dispersions in cyclohexane after storing for more than 6 months at RT: (b) 0.2%Tm; (c) 0.5%Tm; (d) 1%Tm; (e) 2%Tm; (f) 5%Tm.

for the β-$NaYF_4$: 20%Yb,5%Tm sample is rather weak. With the concentration of Yb^{3+} fixed at 20%, as the molar ratio of Tm^{3+} decreases from 5% to 0.2%, the intensities of the emissions at around 360 and 450 nm increase more quickly than those at 475 and 650 nm. This result shows that the increase of Tm^{3+} concentration from 0.2% to 5% tends to quench the blue UC emissions. The same effects of different doping ratios of Tm^{3+} also take place when the molar ratio of Yb^{3+} is fixed at 30% and 40% (see Fig. S4 of the ESI†). As a result, by increasing the doping ratio of Tm^{3+}, the color of the overall emission light can be tuned from bright blue to purple, and to dark red for the β-$NaYF_4$: 20%Yb,0.2–5%Tm nanocrystals (see Fig. 4b–f). As shown in Fig. 4b to f, after mild sonication, those colloid solutions which have been aged for more than half a year can be easily redispersed in cyclohexane showing relatively low scattering effects under the laser beam. The effect of different doping ratios of Yb^{3+} cations is shown in Fig. 5 and Fig S5.† With the molar ratio of Tm^{3+} ions fixed at 0.5% or 1%, the relative intensities of emissions at around 360, 450 and 475 nm gradually increase as the molar ratio of Yb^{3+} increases from 20% to 30% and to 40%, while that at around 650 nm is slightly changed.

2.3. UC emissions of β-$NaYF_4$: Yb,Tm nanocrystals with different sizes. Different particle sizes also result in the differences of relative intensities of each UC emission peak and thus the different overall color of the total UC emissions for the as-obtained β-$NaYF_4$: Yb,Tm nanocrystals. As shown in Fig. 6,

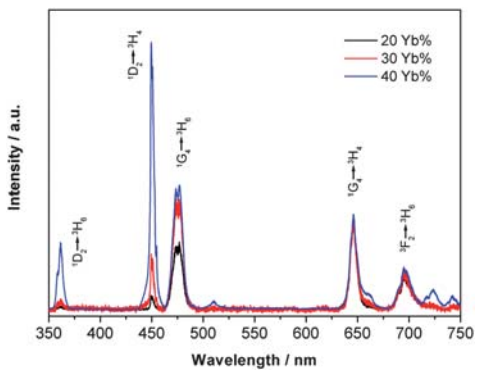

Fig. 5 UC spectra of β-$NaYF_4$: 20–40%Yb,0.5%Tm nanocrystal (~25 nm) dispersion in cyclohexane (1 wt%), normalized at the emission peak of ~650 nm pumped by a 980 nm laser.

when the particle sizes increase from 25 to 50 nm, the relative intensities of UV and blue emission (360 and 450 nm) increase dramatically, while the relative intensities of emissions at 475, 650 and 700 nm would not change so much, and thus the total color would become bluer as a result. When the size of β-$NaYF_4$: 30%Yb,0.5%Tm nanocrystals further increases to about 150 nm with the shape evolution from hexagonal prism to hexagonal plate, the relative intensity of two-photon process (695 nm) decreases significantly, while intensities of the four-photon processes (360 and 450 nm) also drop unexpectedly.

Compared to those smaller nanospheres or nanoprisms, UC properties of large hexagonal plates seem to be more similar to

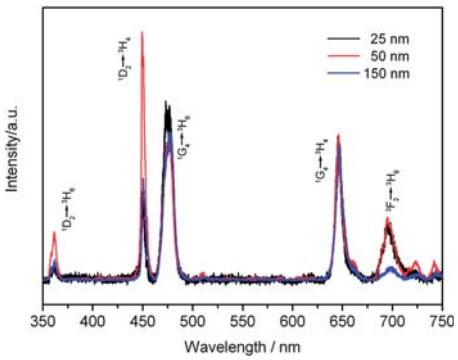

Fig. 6 UC spectra of β-$NaYF_4$: 30%Yb,0.5%Tm nanocrystal dispersions (1 wt%) with different sizes (25–150 nm) pumped by a 980 nm laser.

those of β-$NaYF_4$: Yb,Tm crystals in micro-scale[12] and macro-scale.[2c] In addition, as the particle size increases, the overall intensity of all UC emissions also increases for the as-obtained β-$NaYF_4$: Yb,Tm nanocrystals, resulting in much brighter outcome light which can be seen by naked eyes. The reason for the variation in both relative and total emission intensities observed for the as-obtained β-$NaYF_4$: Yb,Tm nanocrystals was considered to be mainly ascribed to different surface states of nanocrystals with different sizes and shapes, as also revealed in the studies of the UC properties of β-$NaYF_4$: Yb,Er nanocrystals synthesized by similar methods.[8j] On the one hand, larger particle size, *i.e.* smaller surface-to-volume ratio, means the existence of lower density of surface quenching centers and thus leads to the enhanced total UC emissions for the bigger β-$NaYF_4$: Yb,Tm nanocrystals.[8a,j] The unexpected stronger emissions of four-photon process at 360 and 450 nm for ~50 nm β-$NaYF_4$: Yb,Tm nanocrystals than those for the bigger (~150 nm) nanocrystals is interesting. The unexpected stronger four-photon process emissions in smaller β-$NaYF_4$: Yb,Tm nanocrystals is rather interesting. Herein, we assumed that the unexpected UC spectra were caused by different local structures around the photoactive sites with the reduction of crystalline size, the increase of surface-to-volume ratio and the inhomogeneity of dopant ions in relatively small nanocrystals.[7f] As mentioned above, in smaller particles, larger surface-to-volume ratio (s/v) would decrease the total intensity, as well as the relative intensity of emissions from higher energy levels ($^1D_2$ of Tm^{3+}, for example); however, in smaller particles the variation of doped Tm^{3+} concentration in different nanocrystals (see EDS results in Table S2 of the ESI†) would also be more significant than in larger ones and thus there would be some nanocrystals with much lower Tm^{3+} concentrations which could give much stronger emissions from $^1D_2$ to $^3H_6$ as the self quenching of Tm^{3+} ions decreased dramatically,[11b] leading to the bluer emission. In our experiment, we further assumed that, when the particle size increased from about 25 nm ($s/v = 0.24$ nm^{-1}, sphere) to 50 nm ($s/v = 0.12$ nm^{-1}, hexagonal prism), the decreasing of surface-to-volume ratio would play a dominant role in affecting the UC emissions, and the intensity of four-photon process emission would become much stronger. However, when the nanocrystals grew further to ~150 nm hexagonal plates ($s/v = 0.06$ nm^{-1}, 150 nm × 70 nm, hexagonal plates), the decreasing of surface-to-volume ratio would not have obvious influence on the UC spectra as before. While the enhanced doping homogeneity in large nanocrystals would lead to fewer nanocrystals in which the Tm^{3+} doping concentrations were much lower than expected (see EDS results in Table S2 in the ESI†), and then resulted in the decrease of the relative intensity of four photon emissions. In addition, we supposed that as the particle size increased to hundreds of nanometres, the scattering effects of those particles in the colloidal solutions would become much stronger, which may also have strong effects on the acquired UC spectra.

3. UC mechanism of β-$NaYF_4$: Yb,Tm nanocrystals

To confirm the multi-photon processes involved in the UC behaviors of our β-$NaYF_4$: Yb,Tm nanocrystals, we carried out the power density dependent UC measurements. As shown in Fig. 7 and Fig. S3,† we can easily assign the emission bands into different multi-photon transition processes. The ultra-violet emission at about 360 nm and blue emission at about 450 nm are of four-photon processes, that is, the transition from $^1D_2$ to $^3H_6$ and $^3H_4$, respectively. The blue emission at about 475 nm and red emission at about 650 nm are of three-photon processes, $^1G_4$ to $^3H_6$ and $^1G_4$ to $^3H_4$, respectively. And the two-photon UC processes include the emission band of about 695 nm (red, $^3F_3$ to $^3H_6$).

During the characterization of UC emissions of β-$NaYF_4$: 30%Yb,0.5%Tm nanocrystals (23.9 ± 0.8 nm), we found that slopes of intensity–power (*I–P*) curves of near-UV and visible emission bands would decrease, meaning that a UC saturation effect would take place when the excitation power density of the 980 nm laser increased up to a certain value (see Fig. S6 in the ESI†). We considered the decrease of the *I–P* curve slopes to be the result of saturation effects of the intermediate levels of Yb^{3+} and Tm^{3+}(esp. $^2F^{5/2}$ of Yb^{3+}, $^1D_2$, $^1G_4$ and $^3F_4$ of Tm^{3+}), which, as pointed out by Hewes *et al.*,[11a] can be easily affected by heating effects of the NIR laser beam and some other factors.

Our analyzed experiment results (see Fig. 7 and Fig. S2, S3 and S6 in the ESI†) indicate that the transitions from energy level $^1D_2$ to $^3H_6$ (ground state), $^3H_4$ and $^3H_5$ are four-photon processes, transitions from $^1G_4$ to $^3H_6$ and $^3H_4$ are three-photon processes,

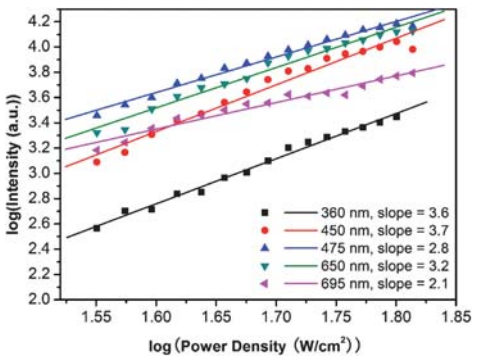

Fig. 7 Power dependence of the UC emissions of β-$NaYF_4$: 30%Yb,0.5%Tm nanocrystal dispersions in cyclohexane (47.3 ± 1.7 nm) (pumped by a 980 nm laser). The straight lines are least-squares fits to the data points.

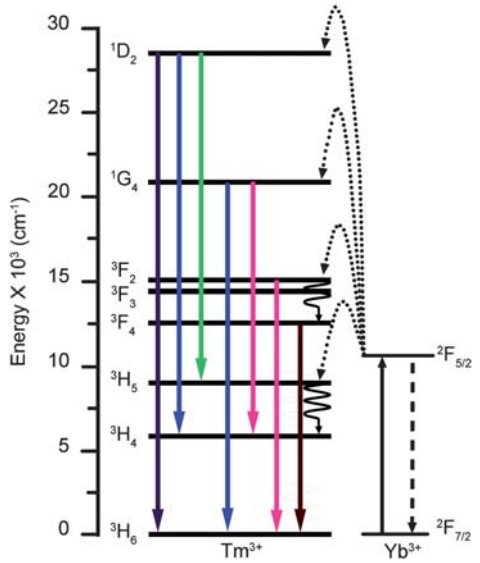

Fig. 8 Schematic energy level diagrams, UC excitation and emission schemes for the $NaYF_4$: Yb,Tm systems, showing two- ($^3F_2$ to $^3H_6$ and $^3F_4$ to $^3H_6$), three- ($^1G_4$ to $^3H_6$ and $^1G_4$ to $^3H_4$) and four-photon ($^1D_2$ to $^3H_6$, $^1D_2$ to $^3H_5$ and $^1D_2$ to $^3H_4$) UC processes (pumped by a 980 nm laser).

and transitions from $^3F_2$, $^3F_3$ and $^3F_4$ to $^3H_6$ are two-photon processes, and thus suggest that the successive transfer model instead of the cooperative sensitization model,[9d] would be more acceptable, as shown in Fig. 8.

As pointed out by Ostermayer *et al.*,[11b] the main factors determining the efficiency of the UC excitations and emissions lie in the Yb-to-Tm transfer probabilities and the quenching of Tm and Yb manifolds. A relatively low ratio of Tm^{3+} (0.03%) and a certain percentage of Yb^{3+} (around 30%) are preferred to get more efficient blue light emissions in bulk YF_3 system. Our results indicate that higher percentage of Tm^{3+} would result in the dramatic reduction of the blue emissions (four-photon process at about 450 nm and three-photon process at about 475 nm) and the red emission at about 650 nm (three-photon process). And as the Tm^{3+} percentage rises to 5%, emissions of shorter wavelengths vanished dramatically, and the sole visible emission band left is the one at about 695 nm (Fig. 4 and Fig. S4 of the ESI†). The reason can be assigned to the self-quenching of Tm^{3+} $^1D_2$ and $^1G_4$ manifolds, which was much more sensitive to the concentration of Tm^{3+} compared to the case of Er^{3+} activated rare earth fluorides.[11b] Thus, as the Tm^{3+} percentage rises from 0.2% to 5%, the total color of the UC emission would turn from bright blue to dark red. Meanwhile, the proper increase of Yb^{3+} concentration would enhance the Yb-to-Tm transfer probabilities, and then result in the enhanced relative intensities of the blue emissions at 450 and 475 nm (especially the one at 450 nm) (see Fig. 5 and Fig. S5†). However, as the ratio of Yb^{3+} increases further, the quenching of Tm^{3+} manifolds by Yb^{3+} would become more significant and the blue emissions would become weaker instead of becoming stronger any more.[11b] Our experiments have proved that β-$NaYF_4$: 40%Yb,0.5%Tm nanocrystals are much better UC materials with blue emissions than β-$NaYF_4$: 20%Yb,0.5%Tm nanocrystals (see Fig. 5). In addition, it is observed with naked eyes that relatively larger β-$NaYF_4$: Yb,Tm nanocrystals would result in brighter UC light due to the less surface defects as well as less influence of surface ligands.[8j]

As discovered above, a relatively low ratio of Tm^{3+} and about 40% or more of Yb^{3+} may result in the brighter and bluer emissions. Maybe a much lower percentage of Tm^{3+} would also lead to the enhancement of UC transitions of Yb^{3+}/Tm^{3+}; however, the segregations of Tm^{3+} cations in different particles would be a big problem in the nano-scale if only trace amount of Tm^{3+} was used in the synthesis procedure. And if for bio-imaging applications, a proper size of the nanocrystals should be chosen in order to balance the intensity of emissions and the colloidal dispersibility of the nanocrystals. Also, we noticed that when the concentration of Yb^{3+} raises to even higher stage, the UC emission process, as well as the mechanism beyond, would be significantly different from those discussed above, which would be one of the issues of our further studies.

Conclusions

Differently-sized, monodisperse, and single-crystalline β-$NaYF_4$: Yb,Tm nanocrystals were obtained by the thermolysis of metal trifluoroacetates in hot surfactant solutions under a controllable and reproducible way. Multicolor UC emissions (blue, purple and red) can be observed for the as-synthesized β-$NaYF_4$: Yb,Tm nanocrystals when excited by a 980 nm CW laser. Through investigating the effects of different concentrations of Tm^{3+} and Yb^{3+} cations and different particle sizes on the UC behaviors of the as-obtained nanocrystals, we found out that relatively low concentrations of Tm^{3+} (*i.e.* 0.2%) and high doping ratios of Yb^{3+} (*i.e.* 40%) were more favored to get purer and brighter blue emissions. We have also deduced the four-, three-, and two-photon processes of the UC excitation and emissions for our β-$NaYF_4$: Yb,Tm nanocrystals, and proved that the successive transfer model instead of the cooperative sensitization model would be applied to account for the UC mechanism of the present nanocrystals. The unexpected stronger emissions of a four-photon process at 360 and 450 nm for ~50 nm β-$NaYF_4$: Yb,Tm nanocrystals than those for the bigger (~150 nm) nanocrystals was observed and explained in terms of the effects of crystallite size, surface-to-volume ratio and homogeneity of the doping cations. In prospect, this work has provided new scientific insights in understanding the fundamental aspects of the size, composition-dependent UC properties and mechanisms of $NaYF_4$: Yb,Tm nanocrystals with blue emissions in the nanometric regime, and promises various nanodevice applications (particularly for bio-imaging and bio-labeling) with the as-synthesized nanocrystalline UC phosphors.

Acknowledgements

We gratefully acknowledge the financial support from the MOST of China (Grant No. 2006CB601104) and NSFC (Grant Nos. 20871006, 20821091, and 20671005).

Notes and references

1 (*a*) F. Auzel, *Chem. Rev.*, 2004, **104**, 139; (*b*) J. F. Suyver, A. Aebischer, D. Biner, P. Gerner, J. Grimm, S. Heer, K. W. Kramer, C. Reinhard and H. U. Güdel, *Opt. Mater.*, 2005, **27**, 1111; (*c*) F. Wang and X. G. Liu, *Chem. Soc. Rev.*, 2009, **38**, 976.

2 (*a*) N. Menyuk, K. Dwight and J. W. Pierce, *Appl. Phys. Lett.*, 1972, **21**, 159; (*b*) J. L. Sommerdijk and A. Bril, *Philips Tech. Rev.*, 1974, **34**, 1; (*c*) K. W. Kramer, D. Biner, G. Frei, H. U. Güdel, M. P. Hehlen and S. R. Luthi, *Chem. Mater.*, 2004, **16**, 1244; (*d*) E. Downing, L. Hesselink, J. Ralston and R. Macfarlane, *Science*, 1996, **273**, 1185; (*e*) M. Huang and F. Meng, *Luminescence*, 2005, **20**, 276.

3 (*a*) S. Sivakumar, F. C. J. M. van Veggel and P. S. May, *J. Am. Chem. Soc.*, 2007, **129**, 620; (*b*) F. van de Rijke, H. Zijlmans, S. Li, T. Vail, A. K. Raap, R. S. Niedbala and H. J. Tanke, *Nat. Biotechnol.*, 2001, **19**, 273; (*c*) G. S. Yi, H. C. Lu, S. Y. Zhao, G. Yue, W. J. Yang, D. P. Chen and L. H. Guo, *Nano Lett.*, 2004, **4**, 2191; (*d*) L. Y. Wang, R. X. Yan, Z. Y. Huo, L. Wang, J. H. Zeng, J. Bao, X. Wang, Q. Peng and Y. D. Li, *Angew. Chem., Int. Ed.*, 2005, **44**, 6054; (*e*) L. Wang and Y. Li, *Chem. Commun.*, 2006, 2557.

4 (*a*) W. N. Millar and L. E. Casida, *Can. J. Microbiol.*, 1970, **16**, 305; (*b*) C. W. Griffin, T. R. Carski and G. S. Warner, *J. Bacterial.*, 1961, **82**, 534; (*c*) J. L. Seifert, R. E. Connor, S. A. Kushon, M. Wang and A. Armitage, *J. Am. Chem. Soc.*, 1999, **121**, 2987; (*d*) C. A. Mirkin, R. L. Letsinger, R. C. Mucic and J. J. Storhoff, *Nature*, 1996, **382**, 607.

5 (*a*) A. P. Alivisatos, K. P. Jonsson, X. G. Peng, T. E. Wilson, C. J. Loweth, M. P. Bruchez and P. G. Schultz, *Nature*, 1996, **382**, 609; (*b*) K. Konig, *J. Microsc.*, 2000, **200**, 83; (*c*) D. R. Larson, W. R. Zipfel, R. M. Williams, S. W. Clark, M. P. Bruchez, F. W. Wise and W. W. Webb, *Science*, 2003, **300**, 1434; (*d*) W. Denk, J. H. Strickler and W. W. Webb, *Science*, 1990, **248**, 73.

6 (*a*) H. J. M. A. Zijlmans, J. Bonnet, J. Burton, K. Kardos, T. Vail, R. S. Niedbala and H. Tanke, *Anal. Biochem.*, 1999, **267**, 30; (*b*) J. A. Feijo and N. Moreno, *Protoplasma*, 2004, **223**, 1; (*c*) S. R. Sershen, S. L. Westcott, N. J. Halas and J. L. West, *J. Biomed. Mater. Res.*, 2000, **51**, 293; (*d*) R. W. Waynant, I. K. Ilev and I. Gannot, *Philos. Trans. R. Soc. London, Ser. A*, 2001, **359**, 635; (*e*) W. C. W. Chan and S. M. Nie, *Science*, 1998, **281**, 2016.

7 (*a*) A. Bril, J. L. Sommerdijk and A. W. De Jager, *J. Electrochem. Soc.*, 1975, **122**, 660; (*b*) J. F. Suyver, J. Grimm, K. W. Kramer and H. U. Güdel, *J. Lumin.*, 2005, **114**, 53; (*c*) J. F. Suyver, J. Grimm, M. K. van Veen, D. Biner, K. W. Kramer and H. U. Güdel, *J. Lumin.*, 2006, **117**, 1; (*d*) L. F. Liang, H. Wu, H. L. Hu, M. M. Wu and Q. Su, *J. Alloys Compd.*, 2004, **368**, 94; (*e*) J. H. Burns, *Inorg. Chem.*, 1965, **4**, 881; (*f*) A. Aebischer, M. Hostettler, J. Hauser, K. Kramer, T. Weber, H. U. Güdel and H. B. Burgi, *Angew. Chem., Int. Ed.*, 2006, **45**, 2802; (*g*) J. F. Suyver, A. Aebischer, S. García-Revilla, P. Gerner and H. U. Güdel, *Phys. Rev. B: Condens. Matter Mater. Phys.*, 2005, **71**, 125123.

8 (*a*) S. Heer, K. Kompe, H. U. Güdel and M. Haase, *Adv. Mater.*, 2004, **16**, 2102; (*b*) J. H. Zeng, J. Su, Z. H. Li, R. X. Yan and Y. D. Li, *Adv. Mater.*, 2005, **17**, 2119; (*c*) H. X. Mai, Y. W. Zhang, R. Si, Z. G. Yan, L. D. Sun, L. P. You and C. H. Yan, *J. Am. Chem. Soc.*, 2006, **128**, 6426; (*d*) J. C. Boyer, F. Vetrone, L. A. Cuccia and J. A. Capobianco, *J. Am. Chem. Soc.*, 2006, **128**, 7444; (*e*) J. C. Boyer, L. A. Cuccia and J. A. Capobianco, *Nano Lett.*, 2007, **7**, 847; (*f*) G. S. Yi and G. M. Chow, *Adv. Funct. Mater.*, 2006, **16**, 2324; (*g*) Y. Wei, F. Lu, X. Zhang and D. Chen, *Chem. Mater.*, 2006, **18**, 5733; (*h*) G. S. Yi and G. M. Chow, *Chem. Mater.*, 2007, **19**, 341; (*i*) L. Y. Wang and Y. D. Li, *Chem. Mater.*, 2007, **19**, 727; (*j*) H. X. Mai, Y. W. Zhang, L. D. Sun and C. H. Yan, *J. Phys. Chem. C*, 2007, **111**, 13721; (*k*) H. X. Mai, Y. W. Zhang, L. D. Sun and C. H. Yan, *J. Phys. Chem. C*, 2007, **111**, 13730; (*l*) F. Zhang, Y. Wan, Y. F. Shi, B. Tu and D. Y. Zhao, *Chem. Mater.*, 2008, **20**, 3778.

9 (*a*) F. Wang and X. G. Liu, *J. Am. Chem. Soc.*, 2008, **130**, 5642; (*b*) H. S. Qian and Y. Zhang, *Langmuir*, 2008, **24**, 12123; (*c*) Z. Q. Li, Y. Zhang and S. Jiang, *Adv. Mater.*, 2008, **20**, 4765; (*d*) O. Ehlert, R. Thomann, M. Darbandi and T. Nann, *ACS Nano*, 2008, **2**, 120; (*e*) M. Nyk, R. Kumar, T. Y. Ohulchanskyy, E. J. Bergey and P. N. Prasad, *Nano Lett.*, 2008, **8**, 3834; (*f*) J. C. Boyer, N. J. J. Johnson and F. C. J. M. van Veggel, *Chem. Mater.*, 2009, **21**, 2010.

10 J. E. Roberts, *J. Am. Chem. Soc.*, 1961, **83**, 1087.

11 (*a*) R. A. Hewes and J. F. Sarver, *Phys. Rev.*, 1969, **182**, 427; (*b*) F. W. Ostermayer Jr., J. P. van der Ziel, H. M. Marcos, L. G. Van Uitert and J. E. Geusic, *Phys. Rev. B: Solid State*, 1971, **3**, 2698.

12 C. X. Li, Z. W. Quan, J. Yang, P. P. Yang and J. Lin, *Inorg. Chem.*, 2007, **46**, 6329.